RESEARCH ARTICLE

NANO · MICRO small
www.small-journal.com

# Role of Curvature-Sensing Proteins in the Uptake of Nanoparticles with Different Mechanical Properties

*Daphne Montizaan, Catherine Saunders, Keni Yang, Sajitha Sasidharan, Sourav Maity, Catharina Reker-Smit, Marc C. A. Stuart, Costanza Montis, Debora Berti, Wouter H. Roos, and Anna Salvati**

**Nanoparticles of different properties, such as size, charge, and rigidity, are used for drug delivery. Upon interaction with the cell membrane, because of their curvature, nanoparticles can bend the lipid bilayer. Recent results show that cellular proteins capable of sensing membrane curvature are involved in nanoparticle uptake; however, no information is yet available on whether nanoparticle mechanical properties also affect their activity. Here liposomes and liposome-coated silica are used as a model system to compare uptake and cell behavior of two nanoparticles of similar size and charge, but different mechanical properties. High-sensitivity flow cytometry, cryo-TEM, and fluorescence correlation spectroscopy confirm lipid deposition on the silica. Atomic force microscopy is used to quantify the deformation of individual nanoparticles at increasing imaging forces, confirming that the two nanoparticles display distinct mechanical properties. Uptake studies in HeLa and A549 cells indicate that liposome uptake is higher than for the liposome-coated silica. RNA interference studies to silence their expression show that different curvature-sensing proteins are involved in the uptake of both nanoparticles in both cell types. These results confirm that curvature-sensing proteins have a role in nanoparticle uptake, which is not restricted to harder nanoparticles, but includes softer nanomaterials commonly used for nanomedicine applications.**

## 1. Introduction

Nanocarriers for drug delivery have high engineering possibilities. Many properties can be tuned to affect their in vivo biodistribution and pharmacokinetic profile, as well as their interaction with cells and subsequent internalization.[1–3] Numerous studies have tried to elucidate how properties such as size, shape, and charge affect nanoparticle uptake efficiency and the endocytic mechanisms involved.[2–5] Recently, the effect of nanoparticle mechanical properties on both their biodistribution and cellular uptake has gained increasing attention.[6–9,10,11] It has for instance been shown that nanoparticle rigidity can affect the uptake rate in macrophages and cancer cells. Most studies indicated that macrophages favor the internalization of more rigid nanoparticles.[6–8,12] The higher uptake of rigid nanoparticles by macrophages is thought to contribute, at least in part, to their shorter circulation time compared to softer nanoparticles.[6] Mixed results have been found, instead, for the

D. Montizaan, C. Saunders[+], K. Yang[++], C. Reker-Smit, A. Salvati
Department of Nanomedicine & Drug Targeting
Groningen Research Institute of Pharmacy
University of Groningen
Antonius Deusinglaan 1, Groningen 9713 AV, The Netherlands
E-mail: a.salvati@rug.nl

The ORCID identification number(s) for the author(s) of this article can be found under https://doi.org/10.1002/smll.202303267

[+]Present address: Department of Materials, Department of Bioengineering, and Institute of Biomedical Engineering, Imperial College London, Exhibition Road, London SW7 2AZ, UK

[++]Present address: Key Laboratory for Nano-Bio Interface Research, Division of Nanobiomedicine, Suzhou Institute of Nano-Tech and Nano-Bionics, Chinese Academy of Sciences, Suzhou 215123, China

S. Sasidharan, S. Maity, W. H. Roos
Molecular Biophysics
Zernike Institute for Advanced Materials
University of Groningen
Nijenborgh 4, Groningen 9747 AG, The Netherlands

M. C. A. Stuart
Electron Microscopy
Groningen Biomolecular Sciences and Biotechnology Institute
University of Groningen
Nijenborgh 7, Groningen 9747 AG, The Netherlands

C. Montis, D. Berti
Department of Chemistry "Ugo Schiff" and CSGI
University of Florence
via della Lastruccia 3, Sesto Fiorentino, Florence 50019, Italy



**DOI: 10.1002/smll.202303267**

ADVANCED SCIENCE NEWS
www.advancedsciencenews.com

NANO · MICRO small
www.small-journal.com



influence of rigidity on nanoparticle uptake by cancer cells.[6,9,10,13–15] Higher uptake of more rigid nanoparticles compared to softer nanoparticles was observed for pegylated lipid-coated polymer nanoparticles on cervical cancer HeLa cells. Similar results were observed when exploring much lower stiffness ranges using hydrogel nanoparticles at different cross linking densities on breast cancer 4T1 cells, and in another work with pegylated polylactide micelles on melanoma A375 cells.[6,9,10] On the other hand, softer nanoparticles entered more than their rigid counterpart in the case of silica nanocapsules on breast cancer MCF-7 cells, and hydrogel nanoparticles on hepatocellular carcinoma HepG2 cells.[13,14] Opposing results were even found when using the same cell-line (HeLa cells), but different nanoparticles systems, thus materials of different properties and different ranges of rigidity.[9,16,17] Palomba et al. suggested that the closer the rigidity of the nanoparticle is to the stiffness of the cell membrane, the lower the internalization.[8] Nanoparticles softer than the cell membrane would deform more easily and take the shape of the membrane wrapping around them, while the stiffer nanoparticles could be repositioned for optimal internalization.[8,18] Clearly, drawing conclusions on the effect of nanoparticle rigidity by comparing the outcomes of these and other similar studies is extremely challenging. Often, outcomes of different studies cannot directly be compared, because not only nanoparticle rigidity is varied, but also many other properties and factors that also affect the uptake mechanism and uptake efficiency, such as nanoparticle material, size, charge, as well as the cells tested and exposure conditions.

Next to similar studies where cells are exposed to nanoparticles of different rigidity to compare their uptake efficiency, computational simulations have provided different insights in the events occurring at the cell membrane when nanoparticles of different mechanical properties interact with lipid membranes and receptors. These studies showed faster membrane wrapping around nanoparticles with higher elasticity, and suggested that because of this, the internalization of harder nanoparticles might be higher than for softer nanoparticles.[9,18,19] Some studies showed deformation and flattening of the softer nanoparticle upon wrapping by a lipid membrane.[9,19–21] Nanoparticle deformation increases the energy requirements for full membrane wrapping, thereby reducing internalization.[19–21] In studies where the nanoparticle volume changed upon deformation, the contact area between the flattened nanoparticle and the membrane enlarged, resulting in increased interactions of nanoparticles with diffusing receptors, thus a decrease in the energy barrier for membrane wrapping.[20,21] On the other hand, in simulations performed by Shen and colleagues using nanoparticle volume constraints, the softer nanoparticles deformed more, but the contact area with the membrane and the number of receptor interactions were similar for nanoparticles with different rigidity. Nevertheless, more nanoparticle–receptor interactions were required to overcome the larger energy barrier for membrane wrapping of the deformed nanoparticle, suggesting a less efficient uptake for softer nanoparticles with a fixed nanoparticle volume.[19]

It is known that inside cells, membrane deformation can be recognized by specific proteins, hereafter called "curvature-sensing proteins." Several curvature-sensing proteins have been implicated in different endocytic pathways.[22–24] A large family of curvature-sensing proteins contains Bin/Amphiphysin/Rvs (BAR) domains.[25,26] Proteins with BAR domains form a curved region upon dimerization and are capable of recognizing different types of curvature, depending on the type of BAR domain.[24,27,28] The binding of BAR domains to negatively charged lipids through electrostatic interactions stabilizes the curvature of the bent membranes and can induce further membrane bending by scaffolding or through insertion of motifs into the lipid bilayer.[25–29] BAR proteins often contain additional domains that facilitate interaction with specific lipids or with proteins involved in endocytosis, such as dynamin and the initiator of actin polymerization N-WASP (neuronal Wiskott-Aldrich syndrome protein).[23,27,30] Thereby, these curvature-sensing BAR proteins also play a role in various steps of multiple endocytic mechanisms, including in the initiation of vesicle formation, vesicle maturation, and vesicle scission.[22,23,30] Another curvature-sensing protein with a known role in endocytosis is Increased Sodium Tolerance 1 (IST1). IST1 is part of the endosomal sorting complex required for transport ESCRT-III, involved in budding of the endosomal membrane to form multivesicular endosomal bodies.[31] Nonetheless, McCullough et al. have shown that a truncated form of IST1 can, together with another ESCRT-III subunit, also propagate tubule formation in the opposite direction (into the cytosol).[32]

Next to these and other similar curvature-sensing proteins, cells can induce membrane curvature by various mechanisms including via scaffold proteins (e.g., clathrin), via rearrangements of the cytoskeleton, via the ESCRT pathway, as well as upon clustering of transmembrane proteins.[22,30,33,34] It is likely that similar mechanisms are activated upon interaction of nanoparticles with the cell membrane, given also that, because of their size and mechanical properties, nanoparticles themselves are able to bend cell membranes, as well as to induce sol–gel transitions and affect other properties upon interactions with lipid membranes.[18,35,36] Nevertheless, the details of the mechanism of membrane curvature generation involved in nanoparticle uptake are largely unknown. In a recent study we demonstrated for the first time that several curvature-sensing proteins do have a role in the uptake of silica nanoparticles and their involvement varies depending on nanoparticle curvature.[37] However, it is not known yet whether the mechanical properties of nanoparticles also affect the activity of these specialized proteins. More specifically we wondered whether curvature-sensing proteins are involved not only in the uptake of harder materials such as the silica used in our previous study, but also for softer nanomaterials, such as those typically used for nanomedicine, i.e., liposomes.

Within this context, in this work, we used liposome and liposome-coated silica (LCS) as a model system to compare uptake and outcomes on cells of two nanoparticles with similar size and surface properties, but different rigidity. Liposomes are known to be soft and deformable, while silica nanoparticles are much harder.[38–40] Particular care was taken in optimizing the nanoparticle preparation to ensure deposition of a lipid bilayer on the silica cores. The two nanoparticles were characterized by a combination of methods, including dynamic light scattering (DLS), zeta potential measurements, cryo transmission electron microscopy (cryo-TEM), high-sensitivity particle flow cytometry and fluorescence correlation spectroscopy (FCS). Atomic force microscopy (AFM) was used to image individual nanoparticles and quantify their deformation at different imaging forces. Then,

 

ADVANCED SCIENCE NEWS
www.advancedsciencenews.com

NANO · MICRO small
www.small-journal.com



the corona formed upon interaction with serum and the uptake kinetics in HeLa cells were determined and compared. Finally, we have explored the role of curvature-sensing proteins in their uptake by silencing the expression of a panel of BAR domain proteins and IST1, known to have a role in different uptake mechanisms. Understanding how nanoparticle mechanical properties affect uptake efficiency by cells and the mechanism of membrane curvature generation involved may provide new ways to optimize nanomedicine design and improve their efficacy.

## 2. Experimental Section

### 2.1. Liposome Preparation

Liposomes were prepared from 1,2-dioleoyl-sn-glycero-3-phosphocholine (DOPC) and cholesterol (Avanti Polar Lipids) dissolved in chloroform and mixed in a 2:1 molar ratio unless mentioned otherwise. The fluorescent lipophilic dye 1,1′-dioctadecyl-3,3,3′,3′-tetramethylindocarbocyanine perchlorate (Dil) (Sigma-Aldrich) was added at 0–1% (mol Dil total mol$^{-1}$) during the optimization and 1% (mol Dil total mol$^{-1}$) in the optimized condition. The chloroform of the lipid mixture was evaporated with nitrogen, and the lipid mixture was dried overnight under vacuum. The lipid film was rehydrated in Dulbecco's Phosphate Buffered Saline (PBS; Gibco) to 5–10 mg lipid mL$^{-1}$ and sonicated for 5 min. To obtain liposomes of uniform size, the mixture underwent 8 freeze-thaw cycles using liquid nitrogen and a water bath at ≈37 °C, and was extruded 21 times through a 100 nm pore polycarbonate membrane using an Avanti Mini-extruder (Avanti Polar Lipids). The lipid concentration after extrusion was assumed to be the same as the lipid concentration after rehydration (unless specified). Results obtained with the Stewart assay in this and in previous studies showed that the final lipid concentration was in fact within 10% of the starting lipid concentration.[41]

### 2.2. Preparation of Liposome-Coated Silica

Sicastar green-fluorescently labeled and unlabeled plain silica of 100 nm diameter were purchased from Micromod Partikel technologie GmbH and used for optimization of the lipid coating and cellular experiments respectively. Liposome-coated silica particles (LCS) were prepared by adding the liposomes to the silica roughly in a 1:1 to 2:1 weight ratio in PBS. Other lipid to silica ratio's and a 5 mM NaCl solution were used during the optimization when indicated in the main text. The mixture was shortly vortexed and sonicated for 10 min at room temperature in a bath sonicator, followed by at least 1-h incubation at room temperature with regular mixing by pipetting. Additional 8 freeze-thaw cycles and 21 passages through a 200 nm pore polycarbonate membrane using Avanti Mini-extruder (Avanti Polar Lipids) were tested during the optimization, but were not included in the final protocol. The excess of liposomes was removed by centrifugation at 10 000 × $g$ for 10 min, removal of the supernatant, and manual resuspension of the pellet in PBS. The washing procedure was repeated twice, and the pellet was resuspended in 100–200 µL PBS after the last centrifugation. The final LCS concentration was determined by measuring the fluorescence of Dil using a SpectraMax Gemini XPS fluorescence plate reader (Molecular Devices) with excitation 544 nm, emission 600 nm, and 570 nm cut-off. A standard curve was made by serial dilution of the Dil-labeled liposomes in PBS.

### 2.3. Nanoparticle Characterization

Hydrodynamic size by dynamic light scattering and zeta potential of the liposomes and LCS were measured on a Malvern Zetasizer Nano ZS (Malvern Instruments) after dispersion in water, PBS and Minimum Essential cell culture Medium (MEM) supplemented with 10% fetal bovine serum (FBS) (hereafter referred to as complete medium, cMEM). The dispersions in 10% FBS were also characterized after incubation at 37 °C and 5% $CO_2$ for different periods of time. Each sample was measured at least twice with a minimum of 10 runs per measurement.

The fluorescence per particle was determined by fluorescence correlation spectroscopy (FCS) using a Leica TCS SP8 confocal microscope (Leica Microsystems GmbH) equipped with a Pico-Quant FCS modulus (PicoQuant). The nanoparticles and an aqueous dispersion of Alexa Fluor 568 for calibration were measured in wells of Lab-Tek Chambered 1.0 Borosilicate Coverglass System (Nalge Nunc International) using a 63× water immersion objective and a DPSS laser with 561 nm excitation. Emission at 571–600 nm was acquired with a Hybrid SMD detector. Specifically, for calibration a 10 nM aqueous solution of Alexa Fluor 568 was employed; for the particles, stock solutions of ≈5 mg mL$^{-1}$ lipid concentration, were diluted to reach a lipid concentration between 0.1 and 0.2 mg mL$^{-1}$ in the wells. The concentration of particles in solution was then determined through FCS. In FCS, the fluctuations in fluorescence intensity over time ($\delta I(t)$) are analyzed with an autocorrelation function. For Brownian motion of a single component in the confocal volume (3D-Gaussian shape), the FCS curves can be modeled according to the following equation:

$$G(\tau) = \frac{< I(t)\, I(t+\tau)}{\langle I(t)\rangle^2} = \frac{1}{\langle N\rangle} \frac{1}{\left(1+\frac{\tau}{\tau_D}\right)} \frac{1}{\left(1+\frac{\tau}{S^2\tau_D}\right)^{\frac{1}{2}}} \quad (1)$$

With $N$, number density of particles; $\tau_D$, particle diffusion time; $S$, the structural parameter of the detection volume ($S = z_0/w_0$ with $w_0$ and $z_0$ lateral and axial parameters, respectively, determined through calibration). From the diffusion time $\tau_D$, the diffusion coefficient of the diffusing species $D$ was calculated using the following equation:

$$\tau_D = \left(w_0^2 + R_h^2\right)/4\, D \quad (2)$$

which is applied if the diffusing objects are of comparable hydrodynamic radius ($R_h$) as the detection volume.[42] Then, from the estimated diffusion coefficient, the hydrodynamic radius was calculated through the Stokes–Einstein equation.

From the number density of particles ($N$) and the structural parameter values estimated from the calibration procedure, the concentration of the diffusing objects in each sample was determined.

$$c = \frac{N}{\pi^{3/2} c w_0^2 z_0} \quad (3)$$

 

ADVANCED SCIENCE NEWS
www.advancedsciencenews.com

NANO · MICRO small
www.small-journal.com



Finally, from FCS data the relative nanoparticles brightness was calculated as the ratio between the average fluorescence intensity of the sample and the concentration of diffusing particles in the same sample, measured in the same experimental conditions.

High-sensitivity flow cytometry was performed using a flow cytometer Cytoflex S (Beckman Coulter) with a 405 nm laser for the detection of side scattering (SSC), a 488 nm laser with a 525/40 nm filter (FITC channel) to detect the green-fluorescently labeled silica and 561 nm laser with a 585/42 nm filter (PE channel) to detect Dil fluorescence in the lipid bilayer. As controls, PBS, liposomes, and bare silica were measured. Samples were highly diluted in PBS to obtain 1000–3500 events $s^{-1}$ and 50 000 events were acquired per sample. The background signal was removed by putting thresholds in the FITC or PE channels for liposome or LCS and silica samples respectively. Liposomes and bare silica were used to gate the particles with double fluorescence (Dil and silica) with FlowJo (version 10).

The lipid coverage of the liposome-coated silica nanoparticles was further characterized by cryo transmission electron microscopy (cryo-TEM). When mentioned in the results, the sample was stained with 1% $OsO_4$ solution in water (Sigma-Aldrich) at a 1:1 volume ratio for 5 min. The LCS were spun down for 1 min at 10 000 × *g* and resuspended in PBS (or NaCl when the LCS were prepared in NaCl for optimization). The sample was loaded on a carbon-coated copper grid (Quantifoil 3.5/1, Quantifoil Micro Tools) (3 µL per grid) and rapidly frozen with liquid ethane using FEI Vitrobot (Thermo Fisher Scientific). Images were acquired under low-dose conditions on a FEI Tecnai T20 cryo-electron microscope (Thermo Fisher Scientific) equipped with a Gatan model 626 cryo-stage operating at 200 keV, and with a slow-scan CCD camera. A rough estimation of the lipid coverage on the silica nanoparticles was performed by counting the fraction of silica nanoparticles on which a lipid bilayer was clearly visible in 4 representative images.

### 2.4. Atomic Force Microscopy

The AFM experiments were performed in liquid environment by quantitative imaging (QI) mode using a JPK Nanowizard ultra-speed AFM. The particles (liposomes or LCS) were immobilized on a poly-L-lysine coated glass coverslip prior to AFM measurements. The poly-L-lysine coated coverslips were prepared by incubating cleaned coverslips in poly-L-lysine solution (0.01 mg $mL^{-1}$) for 1 h, followed by washing with double-distilled water and drying at 37 °C.[43] A volume of 20 µL of the 100-fold diluted stock sample (liposomes or LCS) was loaded on the poly-L-lysine coverslip for the experiments. AFM imaging was performed in the DPBS buffer using a qp-BioAC CB3 probe (Nanosensors) with a spring constant between 0.03 and 0.09 N $m^{-1}$. To determine the deformability of the particle under investigation, the QI images were acquired using varying imaging forces from 50 to 70 pN (in stepwise increments of 5 pN), while the other imaging parameters such as pixel size (128 × 128 $nm^2$) and pixel time (12 ms) were maintained constant.[44] The acquired images were post-processed using the JPK Data processing software version 6.1. As the liposomes were very fragile in nature, only the height data of the particles that survived (i.e., remained in the same position and did not collapse on the surface) at least three consecutive imaging forces were considered for analysis. The error value in the AFM plots represents the standard error of the mean (SEM).

### 2.5. Corona Isolation and Characterization

In order to keep the same ratio of protein to nanoparticle surface area for the isolation of corona-coated nanoparticles as used for cell experiments in cMEM, 500 µg lipid $mL^{-1}$ of liposomes and LCS were incubated in full fetal bovine serum (FBS; Gibco) (roughly corresponding to 40–50 mg $mL^{-1}$ proteins) or roughly 40 mg $mL^{-1}$ proteins from pooled human serum (TCS BioSciences) for 1 h at 37 °C while shaking. Hard corona-coated nanoparticles were isolated by size exclusion chromatography using a Sepharose CL-4B column (Sigma-Aldrich), as described previously.[41] The column was equilibrated with MEM without phenol red (Gibco), which was also used for elution. The presence of liposomes or LCS in the eluted fractions (0.5 mL) was determined by measuring the absorbance of proteins and Dil at 280 nm and 549 nm respectively on a Nanodrop One Microvolume UV–vis Spectrophotometer (Thermo Fisher Scientific). The fractions absorbing at both 280 and 549 nm were pulled together. The final lipid concentration was determined by measuring the fluorescence of Dil with excitation of 544 nm, emission 600 nm, and 570 nm cut-off on a SpectraMax Gemini XPS fluorescence plate reader (Molecular Devices), and comparing it to a standard curve made from the liposome stock.

The protein concentration was determined using the Bio-Rad DC protein assay (Bio-Rad Laboratories, Inc.) according to manufacturer's protocol. Briefly, 25 µL of the reagent $A_S$ was added to 5 µL of sample. After adding 200 µL of reagent B, the sample was incubated 15 min in dark. The absorbance at 700 nm was measured on a Synergy H1 plate reader (BioTek Instruments). A calibration curve made from a serial dilution of BSA in PBS was used to calculate the protein concentration.

Before corona protein separation by gel electrophoresis, corona-coated liposomes were concentrated using cellulose spin filters with a cut-off of 10 kDa (Millipore). The filters were spun at 15000 × *g* and 15 °C till the volume was reduced. Corona-coated LCS were concentrated by centrifugation for 10 min at 15000 × *g* and resuspension of the LCS pellet in a smaller volume of PBS. The final lipid concentration of the concentrated corona-coated liposome and LCS was determined based on the Dil fluorescence as described above. The proteins of the corona from the concentrated liposome and LCS were separated by sodium dodecyl sulfate-polyacrylamide gel electrophoresis (SDS-PAGE). Samples corresponding to 15 µg lipid were mixed with 4× loading buffer (200 mM Tris -HCl, 400 mM DTT, 8% SDS, 0.4% bromophenol blue and 40% glycerol) and boiled for 5 min at 95 °C before loading on a 10% polyacrylamide gel (15 µg lipid per lane). FBS (30 µg) was loaded as a control, and Precision Plus protein all blue standard (Bio-Rad Laboratories, Inc.) as a marker. After running the gel for 90 min at 100 V, the gel was stained for 1 h with 0.1% Coomassie blue R-250 in water/methanol/glacial acetic acid solution (5:4:1, v/v) to visualize the proteins. Excess staining was removed by boiling the gel for 30 min in water and incubating it

 

for at least one day in water. Images were taken with a ChemiDoc XRS (Bio-Rad Laboratories, Inc.).

### 2.6. Cell Culture

Human cervical cancer epithelial HeLa cells (ATCC CCL-2) and lung adenocarcinomic alveolar basal epithelial cells (ATCC CCl-185) were cultured in complete medium (cMEM) consisting of MEM (Gibco) supplemented with 10% FBS (Gibco) at 37 °C and 5% $CO_2$, and split when confluent. Cells were checked monthly to be mycoplasma free, and used until 20 passages after defrosting.

### 2.7. Uptake Kinetics and Sodium Azide

HeLa cells (30 000 cells per well for long uptake kinetics and 50 000 cells per well for $NaN_3$ treatment) were seeded the day before in a 24-well cell-culture plate (Greiner Bio-One). Subsequently, cells were exposed to liposomes or LCS (50 µg $mL^{-1}$ lipid unless specified) in cMEM at 37 °C and 5% $CO_2$ for the indicated times. In case of $NaN_3$ treatment, cells were first incubated 30 min with 5 mg $mL^{-1}$ $NaN_3$ in cMEM, before exposing the cells to the nanoparticle dispersion with 5 mg $mL^{-1}$ $NaN_3$ in cMEM. Untreated cells were used as control.

### 2.8. RNA Interference

The Silencer Select siRNA constructs were purchased from Thermo Fisher Scientific (see Table S2, Supporting Information). Scrambled siRNA (Silencer Select negative control no. 1, Thermo Fisher Scientific) was used as a negative control. The day before RNA interference, 13 000 HeLa or A549 cells were seeded per well of a 24-well cell-culture plate (Greiner Bio-One). For each well, 10 pmol siRNA was mixed with 1 µL Oligofectamine (Life Technologies) in OptiMEM (Gibco) and incubated for 20 min at room temperature. Next, the siRNA-oligofectamine complex was diluted in serum-free MEM to 250 µL and added to cells that were washed once with serum-free medium. After 4–5 h of incubation, MEM with 30% FBS was added to the cells to obtain a final concentration of 10% FBS. After 72 h, cells were exposed for 24 h to freshly isolated FBS or human serum corona-coated liposomes or LCS in serum-free MEM (50 µg lipid $mL^{-1}$), prior to collection for flow cytometry.

### 2.9. Flow Cytometry of Cells

To collect cells for flow cytometry, the nanoparticle dispersion was removed and cells were washed once with cMEM and twice with PBS. Cells were detached by incubation with 0.05% trypsin-EDTA (Gibco) in PBS for 5 min at 37 °C. The trypsin was stopped by addition of cMEM and cells were harvested. The cell suspension was spun 5 min at 300 × $g$ and the cell pellet was resuspended in 100 µL of PBS before flow cytometry measurement on a Cytoflex S (Beckman Coulter, Inc.) or BD FACSArray (BD Biosciences). The fluorescence of the Dil dye was used as a measure for nanoparticle uptake. Cells were gated in a forward scatter area versus side scatter area plot, and single cells were selected in a forward scatter height versus forward scatter area plot. At least 15 000 single cells were acquired per sample. The data were analyzed with FlowJo (version 10; FlowJo, LLC). For each condition, three replicate samples were prepared, unless specified, and experiments were repeated multiple times to confirm the outcomes (as specified in figure captions).

### 2.10. Statistical Methods

The DLS data are depicted as a representative size distribution and the zeta potential is shown as the mean and standard error of the mean over three repeated measurements of the same solution in case of the optimization and over three to four independent preparations after optimization, unless stated otherwise.

The uptake kinetic and sodium azide results are presented in the Supporting Information as the mean with the standard error of the mean (SEM) over three samples in independent replicate experiments. In addition, in Figure 4, in order to compare the results of all experiments, since different instruments were used to measure cell fluorescence, for each experiment the results of the uptake kinetics are normalized for the uptake of the liposomes after 52–53 h exposure, while the sodium azide results are normalized for the uptake in standard conditions (cells exposed to the nanoparticles without sodium azide) after 3 h exposure. A non-parametric Mann–Whitney test was performed in order to compare the normalized uptake levels of all samples in all replicate experiments between the two nanoparticles after 52–53 h exposure and between standard or energy-depleted conditions after 3 h exposure. $p < 0.05$ was considered significant (indicated with *).

For the RNA interference data, the average fluorescence of 3 replicate samples (2 in a few cases) in each independent experiment is depicted together with the mean and standard error of the mean over the three independent experiments. In addition to the average raw data, for each sample in each experiment the uptake in silenced cells is normalized for the average uptake in cells silenced with the negative control siRNA. The normalized results of all replicate samples in all replicate experiments are shown, together with the mean of all values. A non-parametric Kruskal–Wallis test on the normalized results of all samples in all replicate experiments was performed in order to evaluate the overall significance, followed by Dunn's tests to correct for multiple comparisons and identify individual differences in the silenced cells in respect to the control negative siRNA cells. $p < 0.05$ was considered significant (indicated with *). The graphs and statistical analysis were made with Graphpad Prism version 5 and version 9.5.1.

## 3. Results

### 3.1. Nanoparticle Preparation and Characterization

Liposomes and liposome-coated silica (LCS) were selected as a model for nanoparticles of similar size and surface property, but different rigidity. Liposomes of 100 nm were prepared according to a generally described procedure of rehydration of a

 

lipid film and extrusion.[41] In order to prepare liposome-coated silica, as a first step we used rehydration of a lipid film with a silica dispersion.[45,46] However, this led to the formation of large agglomerates (data not shown). Thus, we followed other reported procedures where pre-formed liposomes and silica of the same size (100 nm) are mixed together. It has been shown that mixing silica cores with pre-formed liposomes of comparable size allows efficient deposition of a lipid bilayer onto the silica nanoparticles.[47–50] Thus, as a first step, liposome-coated silica were obtained by sonicating the mixture in order to burst the liposomes open onto the silica nanoparticles. This was followed by additional freeze-thaw cycles to further break the liposomes, and extrusion to reduce the polydispersity of the final liposome-coated silica. Different lipid mixtures were tested to prepare liposomes and ensure efficient coating on the silica nanoparticles (Figure S1, Supporting Information). Additionally, the amount of the labeled lipid DiI in the bilayer was also optimized (Figure S2, Supporting Information). Dynamic light scattering and zeta potential measurements, combined with high-sensitivity particle flow cytometry confirmed that good dispersions of liposome-coated silica could be obtained (Figure S3, Supporting Information). However, quantification of silica and DiI in the final sample showed that upon extrusion a substantial amount of nanoparticles was lost (>80% loss of the initial silica and DiI fluorescence, data not shown). In order to avoid such sample loss, the preparation of liposome-coated silica was further optimized by increasing the incubation time of liposomes and silica at room temperature after sonication, while excluding freeze-thaw cycles and extrusion. Liposome-coated silica prepared in this way in PBS or in 5 mM NaCl (a solution of lower ionic strength), as well as with increasing lipid to silica mass ratio (from 0.5 to 3) were also compared (Figures S4 and S5, respectively, Supporting Information).

Based on these results, we selected the DOPC-Chol liposomes with 1% DiI in PBS and lipid to silica mass ratio of ≈1 as the final conditions and used simple mixing and longer incubation at room temperature (without freeze-thaw cycle and extrusion) to deposit the lipid bilayer onto the silica nanoparticles. In this way, homogenous dispersions of liposome-coated silica with sizes slightly larger than the liposomes, as determined by DLS, and comparable zeta potential could be obtained (**Figure 1**). In order to reduce the presence of liposomes in the LCS sample, the washing steps to remove residual liposomes after bilayer deposition were further optimized. Cryo-TEM imaging showed that with the optimized conditions, almost no empty liposome could be detected, while a lipid bilayer could be observed on most silica nanoparticles (although not quantitative, a rough estimation indicated that out of 108 nanoparticles, only on 8 nanoparticles—roughly 10%—a lipid bilayer was not clearly visible) (Figure 1e). Similarly, high-sensitivity flow cytometry on a sample of green fluorescent silica coated with a red fluorescent lipid bilayer showed that out of 50 000 fluorescent events in the silica channel, roughly 97% of the detected objects showed fluorescence in both channels (Figure 1d). Altogether, these results suggested deposition of bilayers on most silica cores and efficient removal of empty liposomes.

As a next step, for further characterization and comparison of the two nanoparticles, fluorescence correlation spectroscopy (FCS) was used (Figure 1f,g). The average hydrodynamic diameter determined from the diffusion time by FCS was overall slightly larger than the DLS results (Figure 1f,g). This slight difference can be fully attributed to the differences in the experimental methodologies and in the data analysis, as previously reported.[51] The diffusion time of the liposome-coated silica was slightly longer than for the liposomes (consistent with the slightly larger diameter obtained by DLS). Importantly, both liposomes and liposome-coated silica could be analyzed with a single component diffusion, further confirming that no residual liposomes were present in the liposome-coated silica sample after the optimized washing procedure (Figure 1f), as also observed by cryo-TEM (Figure 1e). FCS also allowed us to determine the concentration of the diffusing nanoparticles (which is obtained from the fitting of FCS curve, see Experimental Section for details) (Figure 1g). In this way, we could confirm that nanoparticle numbers were comparable for samples at the same lipid concentration. Similarly, by comparing the concentration of the diffusing nanoparticles with the average fluorescence intensity, we calculated a normalized brightness for each sample, which is an estimate of the relative fluorescence per particle (Figure 1g, see Experimental Section for details). The results showed that the two samples had comparable fluorescence (around 10% difference).

Next, atomic force microscopy (AFM) was used to compare the mechanical properties of the two nanoparticles. A representative topographic image of individual nanoparticles in the two samples is given in **Figure 2**a,b. To characterize the relative nature of deformation, the samples were measured with increasing imaging force.[44] The susceptibility of the two nanoparticles to deformation under increasing imaging force can be quantified by recording their height (Figure 2c–e after normalization and Figure S6, Supporting Information for raw data). The height distribution of the liposomes and liposome coated-silica obtained from AFM imaging (Figure S6, Supporting Information) shows the same trend as the size distribution obtained by DLS (Figure 1b). The fact that the liposomes display a lower height than the average diameter obtained by DLS (Figure 1b) reflects a commonly observed behavior, i.e., that liposomes deform once attaching to a surface.[51] In fact many liposomes already collapsed even when imaging at the lowest force. For the liposomes that survived at least 3 consecutive imaging forces, the results clearly showed strong deformation (see Figure 2e for averaged results and Figure 2f for 3D topographic images of individual liposomes). On the contrary, the liposome-coated silica could be imaged up to 70 pN and their height remained unchanged (Figure 2d,e for the results of individual particles and their average, respectively, and Figure 2f for 3D topographic images). These results confirmed that the two nanoparticles had distinct mechanical properties, with the liposomes relatively softer than the liposome-coated silica.

### 3.2. Cellular Uptake of Liposomes and Liposome-Coated Silica

Having optimized and characterized the two nanoparticles, we then compared their behavior upon exposure to fetal bovine serum, FBS. It is known that proteins and other biomolecules present in the cell culture medium adsorb on the nanoparticle surface forming a corona which can affect nanoparticle stability

 

ADVANCED SCIENCE NEWS
www.advancedsciencenews.com

NANO · MICRO small
www.small-journal.com

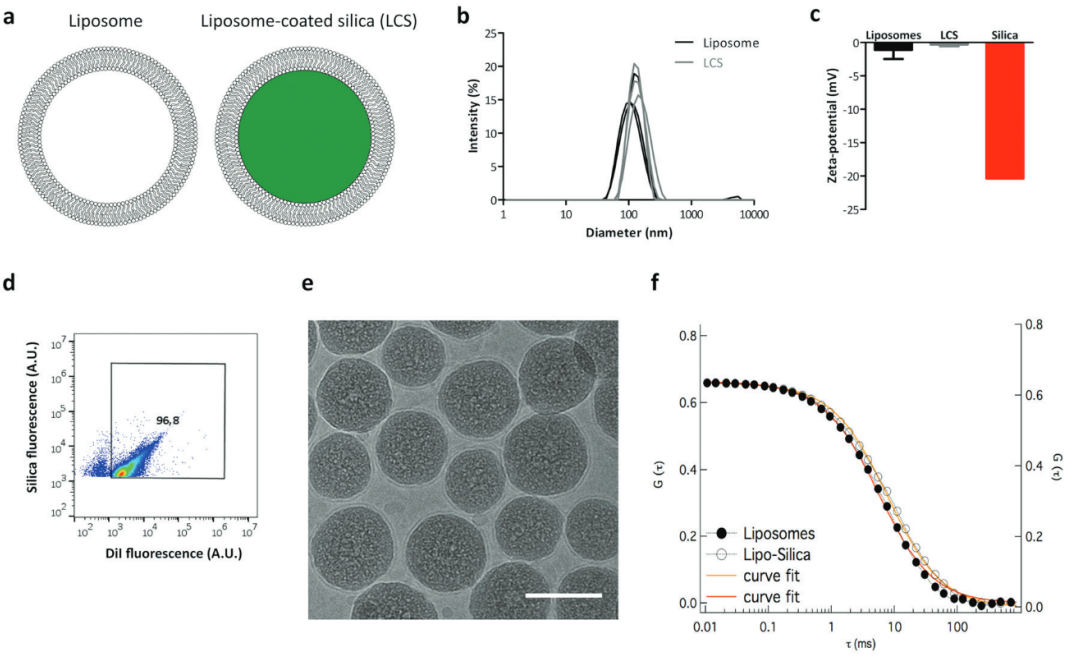


g

| Batch | Nanoparticle | Hydrodynamic diameter by DLS (nm) | Hydrodynamic diameter by FCS (nm) | Average fluorescence (Mcps) | Concentration (nM) | Nanoparticle brightness (Mcps/nM) |
|---|---|---|---|---|---|---|
| 1 | Liposome | 113 ± 4 | 120 ± 20 | 0.75 ± 0.04 | 0.82 ± 0.07 | 0.92 |
| | LCS | 131 ± 4 | 160 ± 20 | 0.83 ± 0.03 | 0.85 ± 0.06 | 0.98 |
| 2 | Liposome | 129 ± 3 | 160 ± 10 | 1.13 ± 0.04 | 2.5 ± 0.1 | 0.46 |
| | LCS | 150 ± 4 | 180 ± 30 | 1.01 ± 0.06 | 2.0 ± 0.2 | 0.50 |

**Figure 1.** Characterization of optimized liposomes and liposome-coated silica. Liposome-coated silica (LCS) were prepared by mixing 100 nm silica nanoparticles with DOPC-Chol liposomes (1% DiI) and sonication (see Experimental Section for details). a) Schematic illustration of the two nanoparticles. b,c) Size distribution by dynamic light scattering (DLS) and zeta potential of liposomes and liposome-coated silica (50 μg $mL^{-1}$ lipid in PBS). For DLS (b), the size distribution of a representative preparation is shown. For zeta potential (c) the average and standard error of the mean of the zeta potential over three independent preparations are shown. (For the silica, instead, the results are the average and standard error of the mean over three measurements of a representative dispersion of 100 μg $mL^{-1}$ silica in PBS.) d) Flow cytometry double scatter plots of liposome-coated silica nanoparticles with DiI in the lipid layer and fluorescently labeled silica cores. Around 97% of the events recorded had double fluorescence. e) Cryo-TEM image of liposome-coated silica, confirming for most silica a coverage with a complete lipid layer. Scale bar, 100 nm. f) Experimental FCS curves of liposomes (filled circles) and LCS (empty circles); curve fit of the experimental curves according to a one component 3D normal diffusion model (continuous lines, see Experimental Section for details). g) From the FCS data, the hydrodynamic diameter, concentration and brightness of the nanoparticles was calculated for two independent preparations (batches). All curves could be analysed with a single component diffusion, suggesting that no residual liposomes were present in the liposome-coated silica sample. Both DLS and FCS showed that liposome-coated silica and liposomes had comparable size, with slightly larger values for the liposome-coated silica. Their zeta potential was also comparable, as was the concentration of nanoparticles (for samples at same mass of lipid) and their brightness estimated from FCS data (see Experimental Section for details).

and interactions with cells.[52,53] Nanoparticle size and charge are known to affect corona formation. However, the effects of nanoparticle mechanical properties on the composition of this layer have not been explored yet.

DLS results showed that both the liposomes and liposome-coated silica did not agglomerate upon exposure to FBS and were stable for at least 24 h at 37 °C (**Figure 3**a). Thus, the corona-coated nanoparticles were isolated using previously optimized methods based on size exclusion chromatography.[41] The same procedure was followed for both nanoparticles to allow direct comparison. DLS confirmed that the isolated corona-coated nanoparticles were well-dispersed and had comparable size and zeta potential (Figure 3b,c, respectively). Quantification of the proteins recovered on the isolated nanoparticle-corona complexes showed that a similar amount of proteins adsorbed on the surface of both liposomes and liposome-coated silica (Figure 3d). Very similar band patterns were obtained for the two samples by SDS-PAGE, suggesting that the corona composition was also comparable (Figure 3e).

We then compared uptake efficiency and kinetics for the two nanoparticles in HeLa cells. These cells were chosen as a common cell model often used both in the nanomedicine and endocytosis fields for similar studies.[9,16,17,37,41] Since FCS confirmed that the fluorescence per particle was similar (within 10% difference) (Figure 1g), the fluorescence of cells after incubation with liposomes or LCS could directly be compared to infer

ADVANCED SCIENCE NEWS
www.advancedsciencenews.com

NANO · MICRO small
www.small-journal.com

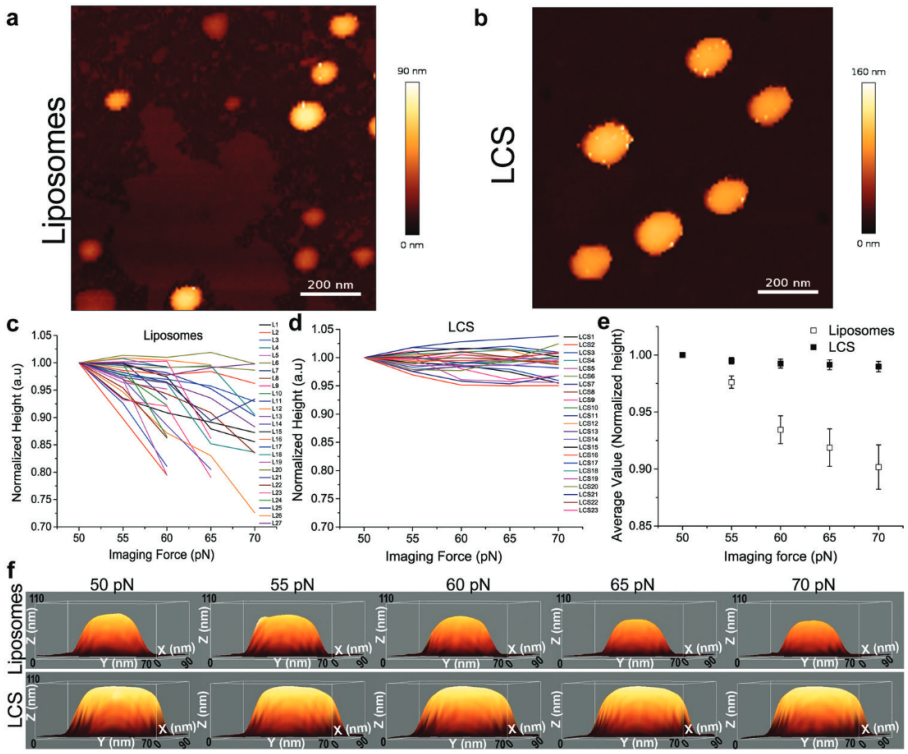


**Figure 2.** Characterization of nanoparticle mechanical properties by AFM. An overview of the topographic image using an imaging force of 50 pN of a) liposomes and b) the liposome-coated silica (LCS). c–e) Characterization of the height of liposomes (c) and liposome-coated silica (d) as a function of the imaging force. The normalized height data of panel (c) represent the population of liposomes that i) remained in place for at least the three consecutive imaging forces of 50, 55, and 60 pN and ii) did not collapse on the surface. The LCS particles instead (d) could be imaged at all imaging forces (50–70 pN). An overall decrease in the height data was observed in the liposomes (c), whereas the LCS particles (d) hardly deformed with an increase in the imaging force. Panels (c) and (d) show the results for individual particles ($N = 27$ and 23, respectively), while panel (e) shows their average and standard error of the mean. f) 3D topographic images of particles at different imaging forces, showing the deformation of the liposomes with an increase in imaging force in comparison to LCS.

relative nanoparticle uptake. The uptake kinetics indicated that liposomes were internalized faster and more than the liposome-coated silica in standard cell culture medium containing FBS (**Figure 4**a for the normalized results and Figure S7, Supporting Information for the corresponding raw data. See Experimental Section for details.). For both nanoparticles, energy depletion by sodium azide strongly reduced uptake, confirming that both nanoparticles entered cells through an active endocytic process (Figure 4b and Figure S7, Supporting Information).

As a next step, in order to determine whether curvature-sensing proteins play a role in the internalization of both nanoparticles and whether their involvement varies for nanoparticles of different mechanical properties, a panel of curvature-sensing proteins was selected and their role in the uptake of the two nanoparticles was studied by silencing their expression using RNA interference. Proteins were selected based on previous observations on their involvement in different endocytic pathways, mainly clathrin-mediated endocytosis (see Table S1, Supporting Information for details). We previously showed that silencing the expression of these proteins with the same RNA constructs in HeLa cells reduced their expression of >80% for most targets (≈60% reduction for BIN2 and FCHO1).[37] Results in standard cell culture medium containing 10% FBS proteins showed little effects on nanoparticle uptake upon silencing (Figure S8, Supporting Information). It is known that free proteins in the serum can compete with nanoparticles thereby reducing their uptake.[55,56] Thus, in order to avoid effects due to the free proteins in solution, FBS corona-coated nanoparticles were first isolated, then the silenced cells were exposed to the corona-coated nanoparticles in a serum free medium. As expected, higher uptake was observed when corona-coated nanoparticles were added to cells in serum-free conditions. The results showed that silencing many of the selected curvature-sensing proteins reduced the uptake of both liposomes and liposome-coated silica to 50–80% (**Figure 5**). Interestingly, however, no major differences were observed in their effects for liposome and liposome-coated silica, despite the different mechanical properties (Figure 2), as well as the different uptake efficiency of the two nanoparticles.

Preliminary studies where nanoparticles were dispersed in a medium with human serum, instead of FBS, showed that also with a human serum corona, in the case of the softer liposomes, several of the selected curvature-sensing proteins had an effect on uptake (Figure S9, Supporting Information). Instead, for the liposome-coated silica the variability across experiments

ADVANCED SCIENCE NEWS
www.advancedsciencenews.com

NANO · MICRO small
www.small-journal.com

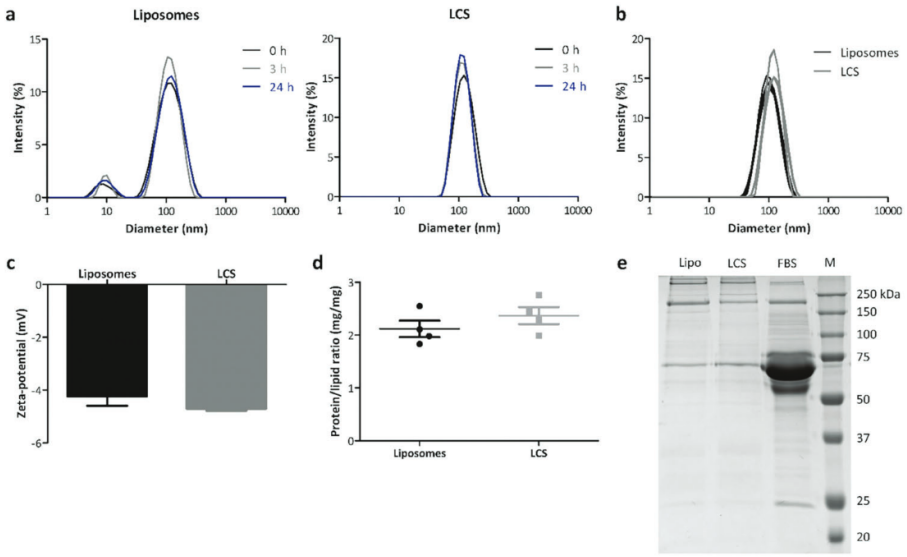


**Figure 3.** Characterization of the liposome and liposome-coated silica in FBS. a) Size distribution by dynamic light scattering (DLS) of liposomes and liposome-coated silica at 100 μg $mL^{-1}$ lipid in complete cell culture medium with 10% FBS after 0, 3, or 24 h of incubation at 37 °C and 5% $CO_2$. Each measurement was repeated three times and the results of a representative measurement are shown. Both liposomes and liposome-coated silica were stable in presence of proteins and up to 24 h in the conditions applied for exposure to cells. A small peak around 10 nm was observed in the liposome samples from the free serum proteins in solution. The corona-coated nanoparticles formed upon exposure to FBS were isolated as described in the Experimental Section. b) Size distribution by DLS and c) zeta potential of isolated corona-coated liposomes and liposome-coated silica (50 μg $mL^{-1}$ lipid in serum-free MEM). The size distribution and the average zeta potential with standard error of the mean over four independent isolations are shown. The isolated corona-coated samples had a similar size and zeta potential for both nanoparticles. d) The protein and lipid amount of the recovered corona-coated liposomes and liposome-coated silica were determined to calculate the relative lipid-to-protein ratio. The average and standard error of the mean over four independent isolations of nanoparticle-corona complexes is presented. Comparable protein amounts were recovered on both samples. e) SDS-PAGE gel image of the proteins recovered in the corona formed on liposome (Lipo) and liposome-coated silica (LCS) (using the same amount of lipid). FBS and a marker (M) were also loaded. The image of a representative SDS-PAGE gel image out of four independent replicate experiments is shown. In all cases a comparable band pattern was observed for the corona proteins of liposomes and liposome-coated silica, with some minor differences in band intensity.

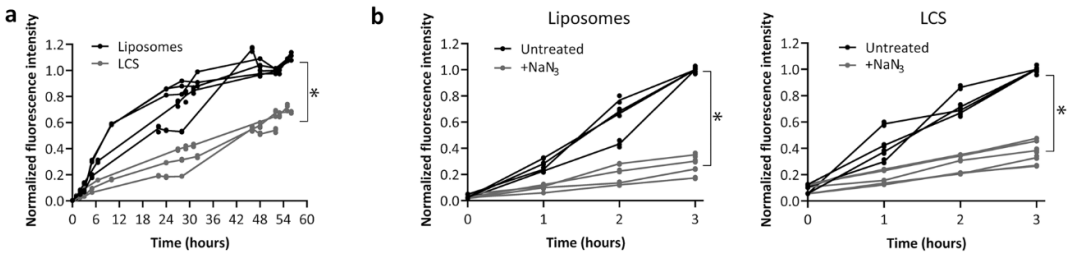


**Figure 4.** Uptake of liposomes and liposome-coated silica by HeLa cells. a) Fluorescence of HeLa cells exposed to 50 μg $mL^{-1}$ lipid of liposomes or of liposome-coated silica (LCS) in complete cell culture medium with 10% FBS (cMEM) as obtained by flow cytometry. b) Fluorescence of HeLa cells exposed to 50 μg $mL^{-1}$ lipid of liposomes or of liposome-coated silica in cMEM in standard conditions (Untreated) or after energy depletion by sodium azide ($NaN_3$) as measured by flow cytometry. For all panels, the results obtained in 3 (panel (a)) or 4 (panel (b)) independent experiments are shown. For each experiment the normalized fluorescence intensity of 3 replicate samples is shown (2 in a few exceptions), together with a line passing through their average. In panel (a) the results of each experiment are normalized for the fluorescence intensity of cells exposed for 52–53 h to the liposomes, while in panel (b), the results are normalized for the fluorescence intensity of cells exposed the nanoparticles for 3 h in standard conditions (untreated, without sodium azide).The corresponding raw values can be found in Figure S7 (Supporting Information). The results indicated that uptake was higher for the liposomes than for liposome-coated silica, and nanoparticles were internalized in an energy-dependent manner. Statistical analysis was performed to compare the normalized uptake levels of the two nanoparticles at 52–53 h exposure (panel (a)) and in standard or energy-depleted conditions at 3 h exposure (panel (b)) using a Mann–Whitney test (see Experimental Section for details). *$p < 0.05$.

ADVANCED SCIENCE NEWS
www.advancedsciencenews.com

NANO · MICRO small
www.small-journal.com



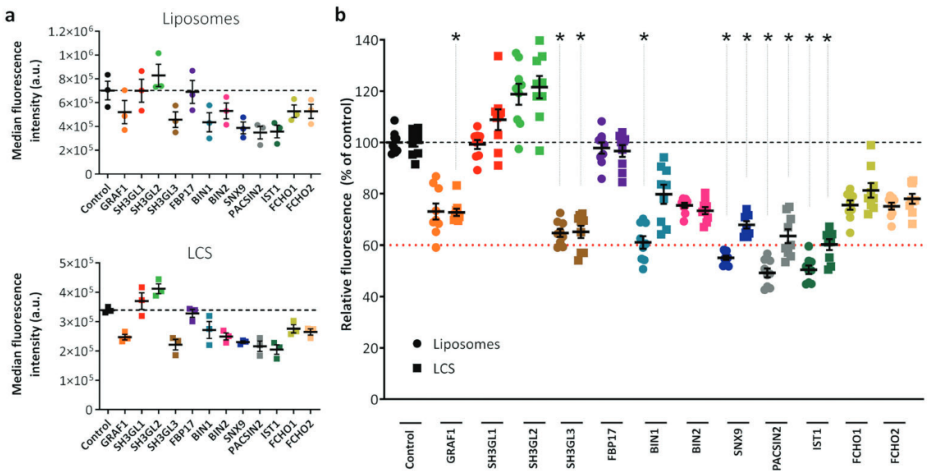


**Figure 5.** Involvement of curvature-sensing proteins in the uptake of liposomes and liposome-coated silica with a FBS corona in HeLa cells. RNA interference was used to silence the expression of a panel of curvature-sensing proteins in HeLa cells, together with a scrambled siRNA as a negative control (Control). Then the corona-coated liposomes and liposome-coated silica (LCS) formed after dispersion in FBS were isolated and their uptake (50 μg $mL^{-1}$ lipids in serum-free MEM) was determined by flow cytometry after 24 h exposure. a) Average and standard error of the mean of the median cell fluorescence intensity obtained in three independent experiments. The dashed line indicates the average fluorescence of control cells exposed to the nanoparticles as a reference. b) The same results of panel (a) are shown after normalization for the uptake in cells transfected with the negative control siRNA. The normalized values of all samples in all replicate experiments are shown together with their mean, indicated by a line, and standard error of the mean. Dashed lines at 100% and 60% uptake are shown as a reference. Statistically significant differences in respect to the uptake in control cells were determined using Kruskal–Wallis test with Dunn's multiple comparison correction (see Experimental Section for details). *$p < 0.05$.

was particularly high. This may suggest variability in the procedure for corona isolation in human serum, which may affect stability and/or interactions with cells. Additionally, in human serum, uptake was higher for the corona-coated complexes formed on liposome-coated silica than for liposomes. Similarly, early tests on cells exposed to the two bare nanoparticles in serum-free medium (without corona) showed that uptake was higher for the liposome-coated silica (Figure S10, Supporting Information).[55,56] Although preliminary, these results suggested that the effect of nanoparticle rigidity on uptake also depends on exposure conditions and the corona formed on the nanoparticles.

Finally, in order to test how these results translate to other cells, similar studies were performed in human A549 lung epithelial cancer cells (**Figure 6**). Also in these cells silencing the expression of some of the tested curvature-sensing proteins reduced nanoparticle uptake, although this was observed for fewer proteins and with smaller effects than what was observed in HeLa cells. Interestingly, in A549 cells, for some of the tested targets such as BIN1 and BIN2, a reduction in uptake was observed only for the liposome-coated silica, suggesting that in these cells they may have a specific role in the uptake of the more rigid nanoparticles. These results further confirmed that curvature-sensing proteins have a role in nanoparticle uptake, but different proteins may be involved depending on the cell type.

## 4. Discussion

Liposome and liposome-coated silica were used a model system to study the cell uptake behavior of two nanoparticles with similar surface properties, but different rigidity. Nanoparticle of different rigidity can be prepared—for instance—by using hydrogels with different cross-linking density. However, with such systems it is often difficult to vary rigidity without affecting also size, charge and shape and the range of stiffness which can be probed is relatively limited.[58,59] Instead, liposomes are typically orders of magnitude softer than silica nanoparticles.[38–40] Thus, by using liposome and liposome-coated silica we could compare the cellular interactions of two nanoparticles of very different mechanical properties, but with same shape and charge, and comparable size.[58,60] Particular efforts were spent in comparing different methods for the preparation of the liposome-coated silica and optimizing the preparation conditions in order to ensure optimal deposition of the lipid bilayer onto the silica cores. After careful optimization, characterization of the final nanoparticles confirmed that with the optimized procedure we could obtain liposome-coated silica with a good bilayer coverage on most nanoparticles, comparable size and zeta potential, and also comparable fluorescence to the liposomes. AFM results confirmed that the two nanoparticles had distinct mechanical properties.

We then explored their stability in serum and compared, to a first qualitative level by SDS-PAGE, their corona composition. Nanoparticle mechanical properties may as well influence interactions with proteins and in this way lead to the formation of a different corona, however this is still an unexplored question. SDS-PAGE showed similar band patterns for the corona proteins recovered from the two samples. However, a deeper analysis, for instance by mass spectrometry, may allow to determine whether more subtle differences in corona composition (which cannot be detected by simple SDS-PAGE analysis) may be present, because of the different mechanical properties.

Next, uptake levels were compared in HeLa cells showing that both nanoparticles entered in an energy-dependent manner, but that liposome uptake was higher than for the more rigid liposome-coated silica. Contrasting results are found

 

ADVANCED SCIENCE NEWS
www.advancedsciencenews.com

NANO · MICRO small
www.small-journal.com

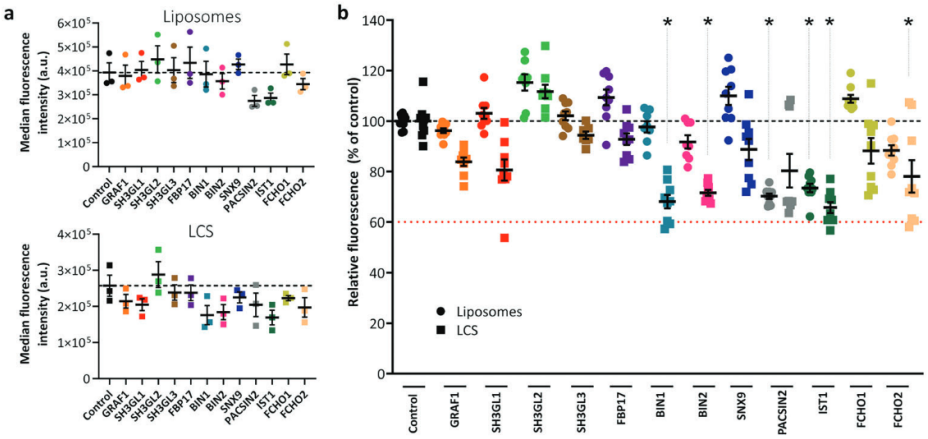


**Figure 6.** Involvement of curvature-sensing proteins in the uptake of liposomes and liposome-coated silica with a FBS corona in A549 cells. RNA interference was used to silence the expression of a panel of curvature-sensing proteins in A549 cells, together with a scrambled siRNA as a negative control (Control). Then the corona-coated liposomes and liposome-coated silica (LCS) formed after dispersion in FBS were isolated and their uptake (50 μg mL$^{-1}$ lipids in serum-free MEM) was determined by flow cytometry after 24 h exposure. a) Average and standard error of the mean of the median cell fluorescence intensity obtained in three independent experiments. The dashed line indicates the average fluorescence of control cells exposed to the nanoparticles as a reference. b) The same results of panel (a) are shown after normalization for the uptake in cells transfected with the negative control siRNA. The normalized values of all samples in all replicate experiments are shown together with their mean, indicated by a line, and standard error of the mean. Dashed lines at 100% and 60% uptake are shown as a reference. Statistically significant differences in respect to the uptake in control cells were determined using Kruskal–Wallis test with Dunn's multiple comparison correction (see Experimental Section for details). *$p < 0.05$.

in literature on the effect of nanoparticle rigidity on uptake efficiency.[6,9,10,13,14] Often, different cells were used, and different cells types are likely to respond differently to changes in nanoparticle rigidity. Even when trying to compare our results to studies using HeLa cells,[9,16,17] other factors affecting uptake by cells are different, including for example nanoparticle material, size, and shape. Additionally, it is important to consider that deformability not only changes with nanoparticle bending modulus, but is also affected by nanoparticle size and shape, making it difficult to compare differently sized and shaped particles with each other.[8,10,19,58,60] In this regard, the system chosen here presents some advantages in that it allows direct comparison of two nanoparticles of comparable size and shape, but different mechanical properties.

As a next step, we tested whether curvature-sensing proteins are involved in the uptake of the two different nanoparticles. We have recently shown that these specialized curvature-sensing proteins are involved in the uptake of silica nanoparticles.[37] While it has been shown that their role varies with nanoparticle size (thus nanoparticle curvature), no information is available as of yet on the effect of nanoparticle mechanical properties on their activity. More specifically, it is not known whether also softer nanomaterials such as those used for most nanomedicine formulations (here represented by the liposomes), may also be able to activate these specialized proteins. Nanoparticle of different mechanical properties may activate a different pool of curvature-sensing proteins at the cell membrane and this could contribute to differences in uptake efficiency (for instance by triggering different uptake mechanisms). Our results demonstrate that curvature-sensing proteins do have a role also in the uptake of softer nanomaterials such as the liposomes. Interestingly, however, in HeLa cells the same curvature-sensing proteins were involved to a similar extent in the uptake of both nanoparticles, despite their different mechanical properties and also the different uptake efficiency (Figure 5). Similar studies in A549 lung epithelial cells confirmed that curvature-sensing proteins do have a role in the uptake of both the liposome-coated silica and the softer liposomes also in these cells (Figure 6). However, in A549 cells some of the tested curvature-sensing proteins seemed to be involved specifically in the uptake of the liposome-coated silica. Several possible explanations can be proposed. In the case of the Hela cells, it is possible that both nanoparticles were relatively rigid compared to the cell membrane and because of this they activated the same curvature-sensing proteins. In A549 cells instead, the fact that different curvature-sensing proteins were involved in the uptake of the two types of nanoparticles suggests that their activation may be modulated by nanoparticle mechanical properties. For both cell types, the different uptake rate could then be due to a difference in membrane wrapping time of the particles because of their different deformability.[9,18,19] Another possible explanation is that, the liposomes and liposome-coated silica entered the cells through different endocytic mechanism, and this may explain the different uptake efficiency. Still, the same curvature sensing proteins could be involved in the uptake by different endocytic mechanisms, since several of these proteins are known to known to have a role in multiple uptake pathways (see Table S1, Supporting Information).[23,26,28,29] Further studies are required to characterize the uptake mechanisms, as well as how these vary depending on nanoparticle mechanical properties.

Another very interesting, though preliminary, observation was that even when using the same cells and nanoparticles, uptake preferences changed when a human serum corona was formed (instead of FBS) or for nanoparticles added to cells in serum-free conditions (Figures S9 and S10, Supporting Information). In these conditions we found higher uptake for the liposome-coated silica. It is known that the serum has a different composition in

 

different species and because of this, exposure of nanoparticles to different sera leads to the formation of different coronas.[57] In turns, when nanoparticles are covered by different coronas, they interact with different receptors on cells, and this can lead to different uptake efficiency, as indeed we observed here.[56] The fact that in both sera silencing the expression of some of the curvature-sensing proteins reduced uptake suggests that these proteins are involved in the uptake mechanism even if receptor interactions and uptake efficiency may differ. It would be important to identify the receptors involved in the two conditions (if present) and more in general how after interactions with receptors or the cell membrane these curvature-sensing proteins participate in the uptake mechanisms.

At a broader level, although preliminary, these results suggested that the effect of nanoparticle rigidity on uptake also depends on exposure conditions and details of the corona formed on the nanoparticles, which ultimately affect the interactions with cell receptors. In line with this, other studies showed that nanoparticle mechanical properties affected the receptor interactions of targeted nanoparticles.[6,61] Anselmo and colleagues observed that modifying pegylated hydrogel nanoparticles (≈200 nm) with anti-ICAM antibodies magnified the difference in uptake between soft and hard particles, with higher uptake for the harder nanoparticle.[6] Similarly, Hui et al. found that attachment of folic acid to pegylated silica nanocapsules (≈150 nm) of different mechanical properties increased the uptake of the rigid nanocapsules more than for the softer nanocapsules by folate-receptor expressing cells, thereby magnifying their difference in uptake efficiency.[61] Further research is required to investigate in more detail the effect of nanoparticle rigidity on both corona composition and targeting in relation to nanoparticle uptake efficiency.

## 5. Conclusion

Overall, using liposomes and liposome-coated silica, this study shows that curvature-sensing proteins play a role in the uptake of nanoparticles of different rigidity, including relatively softer nanomaterials, such as liposomes. Further studies, including computational studies, are needed to understand in more detail how their role varies depending on nanoparticle mechanical properties, for instance by further lowering nanomaterial rigidity by using polymers such as hydrogels. Similarly, our results show that the involvement of these proteins varies depending on the cell type as well as the exposure conditions and the corona formed on the nanoparticles (likely because of interactions with different receptors). Clarifying the role of curvature-sensing proteins in nanoparticle uptake and characterizing the uptake mechanism induced may open up new ways to stimulate nanoparticle uptake into specific targeted cells.

## Supporting Information

Supporting Information is available from the Wiley Online Library or from the author.

## Acknowledgements

This work was funded by the European Research Council (ERC) grant NanoPaths (Grant Agreement No. 637614) and the EU COFUND project oLife (No. 847675). The authors would like to thank Hector Garcia-Romeu for technical support with particle flow cytometry. Henny C. van der Mei (University Medical Center Groningen) is kindly acknowledged for access to Malvern Nanosizer.

## Conflict of Interest

The authors declare no conflict of interest.

## Author Contributions

D.M. supervised particle preparation and characterization, performed the particle corona studies and most experiments on cells and wrote the manuscript, C.S. prepared and characterized the particles and performed initial studies on cells, K.Y. performed initial studies on particle preparation and supervised particle preparation and characterization, S.S., S.M. ,and W.H.R. performed and supported AFM imaging, analysis and interpretation, C.R.S. performed silencing studies in A459 cells and for nanoparticles in human serum, M.C.A.S. performed cryo-TEM imaging and analysis, C.M. and D.B. performed FCS experiments and analysis, A.S. conceptualized and supervised all study and wrote the manuscript. All authors have reviewed and edited the manuscript.

## Data Availability Statement

The data that support the findings of this study are available from the corresponding author upon reasonable request.

## Keywords

curvature-sensing proteins, liposome-coated silica, membrane curvature generation, nanoparticle rigidity, nanoparticle uptake

Received: April 18, 2023
Published online: May 26, 2023

[1] E. Blanco, H. Shen, M. Ferrari, *Nat. Biotechnol.* **2015**, *33*, 941.
[2] R. A. Petros, J. M. DeSimone, *Nat. Rev. Drug Discov.* **2010**, *9*, 615.
[3] X. Duan, Y. Li, *Small* **2013**, *9*, 1521.
[4] B. Yameen, W. I. Choi, C. Vilos, A. Swami, J. Shi, O. C. Farokhzad, *J. Controlled Release* **2014**, *190*, 485.
[5] H. Herd, N. Daum, A. T. Jones, H. Huwer, H. Ghandehari, C.-M. Lehr, *ACS Nano* **2013**, *7*, 1961.
[6] A. C. Anselmo, M. Zhang, S. Kumar, D. R. Vogus, S. Menegatti, M. E. Helgeson, S. Mitragotri, *ACS Nano* **2015**, *9*, 3169.
[7] J. Key, A. L. Palange, F. Gentile, S. Aryal, C. Stigliano, D. Di Mascolo, E. De Rosa, M. Cho, Y. Lee, J. Singh, P. Decuzzi, *ACS Nano* **2015**, *9*, 11628.
[8] R. Palomba, A. L. Palange, I. F. Rizzuti, M. Ferreira, A. Cervadoro, M. G. Barbato, C. Canale, P. Decuzzi, *ACS Nano* **2018**, *12*, 1433.
[9] J. Sun, L. Zhang, J. Wang, Q. Feng, D. Liu, Q. Yin, D. Xu, Y. Wei, B. Ding, X. Shi, X. Jiang, *Adv. Mater.* **2015**, *27*, 1402.
[10] T. Stern, I. Kaner, N. Laser Zer, H. Shoval, D. Dror, Z. Manevitch, L. Chai, Y. Brill-Karniely, O. Benny, *J. Controlled Release* **2017**, *257*, 40.
[11] D. Vorselen, S. M. van Dommelen, R. Sorkin, M. C. Piontek, J. Schiller, S. T. Döpp, S. A. A. Kooijmans, B. A. van Oirschot, B. A. Versluijs, M. B. Bierings, R. van Wijk, R. M. Schiffelers, G. J. L. Wuite, W. H. Roos, *Nat. Commun.* **2018**, *9*, 4960.
[12] K. A. Beningo, Y.-l. Wang, *J. Cell Sci.* **2002**, *115*, 849.
[13] Z. Teng, C. Wang, Y. Tang, W. Li, L. Bao, X. Zhang, X. Su, F. Zhang, J. Zhang, S. Wang, D. Zhao, G. Lu, *J. Am. Chem. Soc.* **2018**, *140*, 1385.

 

[14] W. Liu, X. Zhou, Z. Mao, D. Yu, B. Wang, C. Gao, *Soft Matter* **2012**, *8*, 9235.
[15] P. Guo, D. Liu, K. Subramanyam, B. Wang, J. Yang, J. Huang, D. T. Auguste, M. A. Moses, *Nat. Commun.* **2018**, *9*, 130.
[16] H. Sun, E. H. H. Wong, Y. Yan, J. Cui, Q. Dai, J. Guo, G. G. Qiao, F. Caruso, *Chem. Sci.* **2015**, *6*, 3505.
[17] R. Hartmann, M. Weidenbach, M. Neubauer, A. Fery, W. J. Parak, *Angew. Chem., Int. Ed.* **2015**, *54*, 1365.
[18] X. Yi, X. Shi, H. Gao, *Phys. Rev. Lett.* **2011**, *107*, 098101.
[19] Z. Shen, H. Ye, X. Yi, Y. Li, *ACS Nano* **2019**, *13*, 215.
[20] Z. Shen, H. Ye, Y. Li, *Phys. Chem. Chem. Phys.* **2018**, *20*, 16372.
[21] X. Yi, H. Gao, *Nanoscale* **2017**, *9*, 454.
[22] V. Haucke, M. M. Kozlov, *J. Cell Sci.* **2018**, *131*.
[23] M. Sathe, G. Muthukrishnan, J. Rae, A. Disanza, M. Thattai, G. Scita, R. G. Parton, S. Mayor, *Nat. Commun.* **2018**, *9*, 1835.
[24] H. T. McMahon, E. Boucrot, *J. Cell Sci.* **2015**, *128*, 1065.
[25] B. J. Peter, H. M. Kent, I. G. Mills, Y. Vallis, P. J. G. Butler, P. R. Evans, H. T. McMahon, *Science* **2004**, *303*, 495.
[26] H. T. McMahon, J. L. Gallop, *Nature* **2005**, *438*, 590.
[27] P. J. Carman, R. Dominguez, *Biophys. Rev.* **2018**, *10*, 1587.
[28] A. Frost, V. M. Unger, P. De Camilli, *Cell* **2009**, *137*, 191.
[29] L. Johannes, R. G. Parton, P. Bassereau, S. Mayor, *Nat. Rev. Mol. Cell Biol.* **2015**, *16*, 311.
[30] T. Itoh, K. S. Erdmann, A. Roux, B. Habermann, H. Werner, P. De Camilli, *Dev. Cell* **2005**, *9*, 791.
[31] J. McCullough, A. Frost, W. I. Sundquist, *Annu. Rev. Cell Dev. Biol.* **2018**, *34*, 85.
[32] J. McCullough, A. K. Clippinger, N. Talledge, M. L. Skowyra, M. G. Saunders, T. V. Naismith, L. A. Colf, P. Afonine, C. Arthur, W. I. Sundquist, P. I. Hanson, A. Frost, *Science* **2015**, *350*, 1548.
[33] L. Johannes, S. Mayor, *Cell* **2010**, *142*, 507.
[34] A. Bertin, N. de Franceschi, E. de la Mora, S. Maity, M. Alqabandi, N. Miguet, A. di Cicco, W. H. Roos, S. Mangenot, W. Weissenhorn, P. Bassereau, *Nat. Commun.* **2020**, *11*, 2663.
[35] B. Wang, L. Zhang, S. C. Bae, S. Granick, *Proc. Natl. Acad. Sci. U. S. A.* **2008**, *105*, 18171.
[36] G. Rossi, J. Barnoud, L. Monticelli, *J. Phys. Chem. Lett.* **2014**, *5*, 241.
[37] V. Francia, C. Reker-Smit, A. Salvati, *Nano Lett.* **2022**, *22*, 3118.
[38] F. W. S. Stetter, T. Hugel, *Biophys. J.* **2013**, *104*, 1049.
[39] O. Et-Thakafy, N. Delorme, C. Gaillard, C. Mériadec, F. Artzner, C. Lopez, F. Guyomarc'h, *Langmuir* **2017**, *33*, 5117.
[40] M. Zou, D. Yang, *Tribol. Lett.* **2006**, *22*, 189.
[41] K. Yang, B. Mesquita, P. Horvatovich, A. Salvati, *Acta Biomater.* **2020**, *106*, 314.
[42] K. Koynov, H.-J. Butt, *Curr. Opin. Colloid Interface Sci.* **2012**, *17*, 377.
[43] D. Vorselen, M. C. Piontek, W. H. Roos, G. J. L. Wuite, *Front. Mol. Biosci.* **2020**, *7*, 139.
[44] M. Alqabandi, N. de Franceschi, S. Maity, N. Miguet, M. Bally, W. H. Roos, W. Weissenhorn, P. Bassereau, S. Mangenot, *BMC Biol.* **2021**, *19*, 66.
[45] H. Meng, M. Wang, H. Liu, X. Liu, A. Situ, B. Wu, Z. Ji, C. H. Chang, A. E. Nel, *ACS Nano* **2015**, *9*, 3540.
[46] R. T. Ribeiro, V. H. A. Braga, A. M. Carmona-Ribeiro, *Biomimetics* **2017**, *2*, 20.
[47] P. N. Durfee, Y.-S. Lin, D. R. Dunphy, A. J. Muñiz, K. S. Butler, K. R. Humphrey, A. J. Lokke, J. O. Agola, S. S. Chou, I. M. Chen, W. Wharton, J. L. Townson, C. L. Willman, C. J. Brinker, *ACS Nano* **2016**, *10*, 8325.
[48] S. Mornet, O. Lambert, E. Duguet, A. Brisson, *Nano Lett.* **2005**, *5*, 281.
[49] S. Savarala, S. Ahmed, M. A. Ilies, S. L. Wunder, *ACS Nano* **2011**, *5*, 2619.
[50] H. Wang, J. Drazenovic, Z. Luo, J. Zhang, H. Zhou, S. L. Wunder, *RSC Adv.* **2012**, *2*, 11336.
[51] C. Montis, A. Zendrini, F. Valle, S. Busatto, L. Paolini, A. Radeghieri, A. Salvatore, D. Berti, P. Bergese, *Colloids Surf., B* **2017**, *158*, 331.
[52] D. Vorselen, F. C. MacKintosh, W. H. Roos, G. J. L. Wuite, *ACS Nano* **2017**, *11*, 2628.
[53] A. E. Nel, L. Madler, D. Velegol, T. Xia, E. M. V. Hoek, P. Somasundaran, F. Klaessig, V. Castranova, M. Thompson, *Nat. Mater.* **2009**, *8*, 543.
[54] M. P. Monopoli, C. Åberg, A. Salvati, K. A. Dawson, *Nat. Nano* **2012**, *7*, 779.
[55] J. A. Kim, A. Salvati, C. Åberg, K. A. Dawson, *Nanoscale* **2014**, *6*, 14180.
[56] V. Francia, K. Yang, S. Deville, C. Reker-Smit, I. Nelissen, A. Salvati, *ACS Nano* **2019**, *13*, 11107.
[57] K. Yang, C. Reker-Smit, M. C. A. Stuart, A. Salvati, *Adv. Healthcare Mater.* **2021**, *10*, 2100370.
[58] Y. Hui, X. Yi, F. Hou, D. Wibowo, F. Zhang, D. Zhao, H. Gao, C.-X. Zhao, *ACS Nano* **2019**, *13*, 7410.
[59] L. Ribovski, E. de Jong, O. Mergel, G. Zu, D. Keskin, P. van Rijn, I. S. Zuhorn, *Nanomedicine* **2021**, *34*, 102377.
[60] A. C. Anselmo, S. Mitragotri, *Adv. Drug Deliv. Rev.* **2017**, *108*, 51.
[61] Y. Hui, D. Wibowo, Y. Liu, R. Ran, H.-F. Wang, A. Seth, A. P. J. Middelberg, C.-X. Zhao, *ACS Nano* **2018**, *12*, 2846.